Field Emission with Ultralow Turn On Voltage from Metal Decorated Carbon Nanotubes

Srividya Sridhar,[†] Chandrasekhar Tiwary,[‡,#] Soumya Vinod,[‡] Jose Jaime Taha-Tijerina,[‡] Srividvatha Sridhar,[§] Kaushik Kalaga,[‡] Benjamin Sirota,[∥] Amelia H. C. Hart,[‡] Sehmus Ozden,[‡] Ravindra Kumar Sinha,[†] Harsh,[⊥] Robert Vajtai,[‡] Wongbong Choi,[∥] Krisztián Kordás,[▽] and Pulickel M. Ajayan[‡,*]

[†]Department of Applied Physics, Delhi Technological University (Formerly Delhi College of Engineering), Bawana Road, Delhi 110042, India, [‡]Department of Materials Science and NanoEngineering, Rice University, Houston, Texas 77005, United States, [§]Department of Chemical and Biomolecular Engineering, Rice University, Houston, Texas 77005, United States, [⊥]Department of Physics, Jamia Millia Islamia, New Delhi 110025, India, [∥]Department of Material Science and Engineering, University of North Texas, Denton, Texas 76203, United States, [#]Materials Engineering, Indian Institute of Science, Bangalore, Karnataka 560012, India, and [▽]Microelectronics and Materials Physics Laboratories, Department of Electrical Engineering, University of Oulu, P.O. Box 4500, FI-90014 Oulu, Finland

ABSTRACT A simple and scalable method of decorating 3D-carbon nanotube (CNT) forest with metal particles has been developed. The results observed in aluminum (Al) decorated CNTs and copper (Cu) decorated CNTs on silicon (Si) and Inconel are compared with undecorated samples. A significant improvement in the field emission characteristics of the cold cathode was observed with ultralow turn on voltage ($E_{to} \sim 0.1$ V/μm) due to decoration of CNTs with metal nanoparticles. Contact resistance between the CNTs and the substrate has also been reduced to a large extent, allowing us to get stable emission for longer duration without any current degradation, thereby providing a possibility of their use in vacuum microelectronic devices.

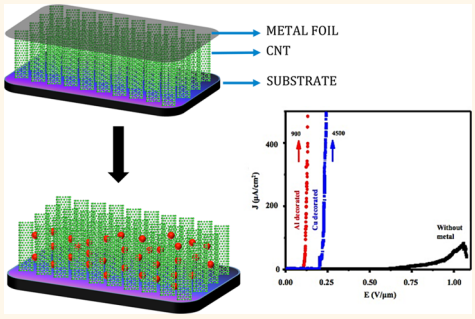

KEYWORDS: field emission · metal decoration · screening effect · work function · edge effect

Because of the high aspect ratio, high mechanical strength and high thermal conductivity, CNTs are considered to be an ideal electron emitting sources in field emission displays.[1−8] Aligned and well-separated CNT cathode morphology is important for many potential applications where a high electric-field is needed, such as in field emission devices. The growth in these cases is usually achieved by chemical vapor deposition (CVD). However, the highly dense growth of CNTs by thermal CVD method may compromise the field emission properties, due to a field-screening effect caused by the proximity of neighboring tubes. Also some critical issues such as adhesion of CNTs with the substrate, reliability, and stability have to be addressed while using CNTs as electron emitters in field emission applications. To improve the field emission performance from CNT emitters, different methods such as doping of CNTs with nitrogen,[9,10] surface coatings with low work function materials such as LaB_6 or Ha for low turn on field[11,12] and decorations with ZnO and Ru[13−15] have been investigated. Previous studies have also shown that tuning the structure of the CNTs such as the radius,[16] geometry,[17,18] structural change by oxygen plasma treatment[19] and improving their density[20] could improve the field emission property. Also by decorating the CNT walls with organic functional groups[21−23] or by inorganic semiconductor[24−31] the field emission properties of CNTs could be enhanced. Chi *et al.*[32] reported a threshold field of 0.9 V/ μm at 1 mA/cm^2, which correlated to a turn on voltage of 0.6 V/μm at 10 μA/cm^2 by growing CNTs on a mesh electrode. Also, Zuo *et al.*[33] demonstrated low turn on field of 0.63 V/μm at 10 μA/cm^2 by decorating the surface of the CNT with titanium nanoparticles. Pandey *et al.*[34] arrived at a threshold field of 0.8 V/μm in strontium titanate coated CNTs. On the other hand, Liu *et al.*[15] decorated CNTs with Ru nanoparticle and the turn on field reduced from 2.5 to 1.3 V/μm after Ru decoration. In the recent report of Zannin

* Address correspondence to ajayan@rice.edu.

Received for review February 15, 2014 and accepted July 15, 2014.

Published online July 15, 2014
10.1021/nn500921s

et al.[35] hybrid diamond-like carbon and CNT composite structures showed threshold field of 2 V/μm. Thus, to the best of our knowledge, such low turn on field of 0.1 V/μm achieved in this work has not been reported so far.

Electrophoretic deposition (EPD) technique is a common method used for decorating the CNTs with the desired metal particle to improve the field emission properties of the cold cathode.

Fan *et al.*[36] used CNT/Ni composite and Chen *et al.*[37] fabricated CNT/Cu composite to enhance the field emission properties of the CNTs. But during the fabrication, the CNTs in the composites would be easily covered by the deposited nanoparticles in the chemical process resulting in the decrease of effective field emitters in the CNT cathode. Another important issue of CNTs getting bundled together is also common in this process. Once they are bundled, without the use of aggressive treatment like ultrasonication or chemical functionalization, it is extremely difficult to achieve a stable dispersion or homogeneous mixture. These measures are known to damage the walls of the CNTs and degrade their electrical properties to a larger extent. Moreover, this process cannot alter the distance between the CNTs. Although it is important to lower the turn on and threshold voltage for better field emission results, reducing the screening effect is crucial for CNTs to be used in field emission application. It is well-known that if the separation between the tubes, *d*, is much less than the tube height, *h*, in an array, the electrostatic shielding between the CNTs can drastically affect the field emission performance of the cold cathode. Numerical simulations show that if the distance between the CNTs is equal to or more than twice the height of the CNTs, then the screening effect can be considerably reduced which in turn could improve the field emission property of the cathode.[38−40] Electrostatic shielding becomes a significant hurdle for future device applications because of the exponential dependence of the emission current on the electric field in accordance with the Fowler-Nordheim theory. Work has also been done on thermally evaporated nanoparticles on nanotubes.[41−43] The results in these work indicate that the morphology of the metal particle or the film on the CNTs is dependent on the intrinsic properties of the metal themselves than on the process parameters. On the other hand, the work of Muratore *et al.*[44] reported the effect of particle growth temperature and time on the decorated metal nanoparticles' density and morphology. However, the sputtered metal nanoparticles were attached to the surface of the CNTs without penetrating in between the CNTs to change the inter tubular spacing of those.

The current paper proposes a simple and scalable procedure for decorating the vertically aligned CNTs forest with metal nanoparticles for improved field emission properties. This process enabled the CNTs to bundle toward a metal particle forming a pattern due to which the CNT bundles are separated by almost 3 times the height of the bundle reducing the screening effect considerably. Further, by the deposition of metal nanoparticles on the surface of the nanotubes, emitting centers are obtained that ensure highly conductive paths for the electrons from the nanotubes toward the vacuum helping bypass the amorphous carbon impurities, known as one of the major hurdles in CNT based emitters.

RESULTS AND DISCUSSION

Figure 1a shows the scanning electron microscope (SEM) images of the multiwalled carbon nanotubes (MWCNTs) grown on Si with Al decoration on them. Before the metal decoration, the CNTs were vertically aligned *via* self-supporting mechanism as described in our previous work,[45] due to extremely high density of CNTs. Interestingly, after metal evaporation, the morphology of the CNTs changed completely. Groups of CNTs became linked together by their tips while attaching to the Al particles forming microscopic patterns in the nanotube forest. Accordingly, the CNTs are no longer individual strands for field emission; instead they are individual bundles. Choi *et al.*[20] also observed similar morphology by H_2 plasma treatment. The surface morphology of vertically aligned MWCNTs changed from flat surface to sharp conical stacks of CNTs due to the post plasma treatment. They claimed that there was improvement in the field emission properties of the CNTs due to the formation of such stacks.

Figure S1a,b (Supporting Information) shows the distribution histogram of the number of CNTs with their height and the number of CNT bundles with the interbundle distance, respectively. From the histogram, it is very clear that most of the CNT bundles are of around 2 μm in their height with inter bundle distances varying mostly between 3 and 5 μm. It is to be noted that bundled CNTs have the advantage of realizing the ideal ratio of inter tube distance to the height for achieving maximum field emission by reducing charge screening effects in adjacent CNTs in the forest.[46] According to Suh *et al.*[47] the field emission would be optimum when the tube height is similar to the intertube distance, while the results of Ren *et al.*[48] suggest 3-fold intertube distance in reference to CNT height to achieve maximum emitter efficiency. In our case, since most of the CNT bundles are separated by almost 3 times the height of the bundle and the bundle are emitting as a whole, the screening effect is reduced considerably and the emitter efficiency has increased substantially. Figure 1b corresponds to the SEM images of Al decorated CNTs grown on Inconel. SEM images clearly show that the CNTs on Inconel are also no longer a uniform film after the metal deposition, however the surface texture of the forests are not the same as for the

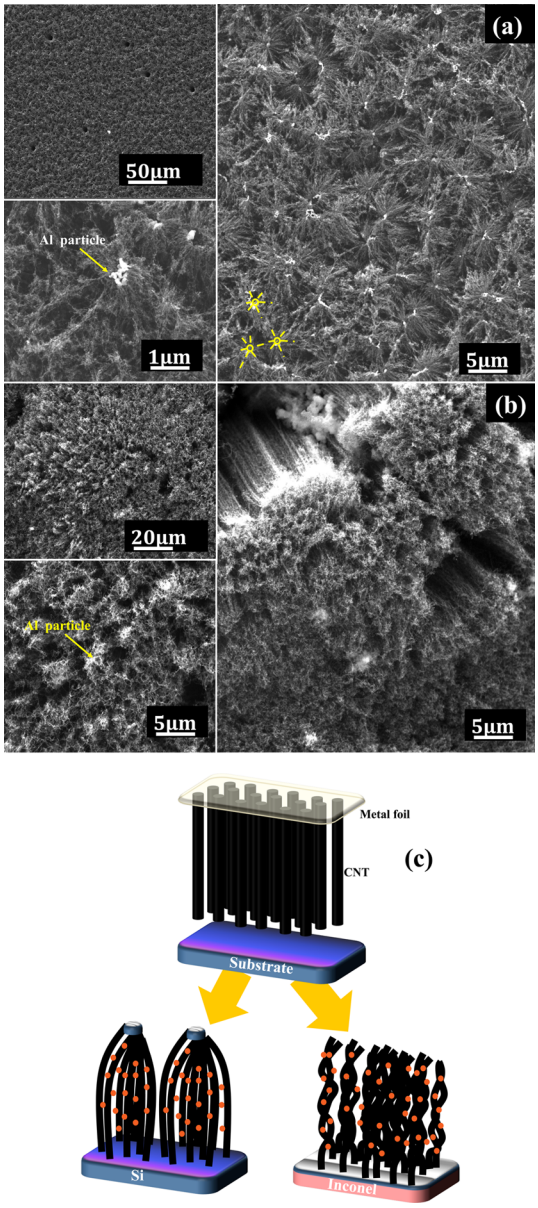

Figure 1. (a) SEM image of CNTs grown on Si with Al decoration in different magnification. SEM image shows the way in which the CNTs got attached to Al particle forming a beautiful pattern. (b) SEM image of the CNTs grown on Inconel with Al decoration on them in different magnification. (c) The schematic procedure for the fabrication of metal decorated CNTs.

other CNTs grown on the other substrate material. The nanotubes in this case formed bundles which reduced the screening effect. A schematic of the morphology of CNTs grown on Si and Inconel substrate is shown in Figure 1c. Although the mechanisms responsible for the differing surface textures after evaporating the metals on the different films are not clear, a number of different reasons associated with the wetting behavior of the CNT forests with the molten metal (and/or with the condensing metal from the vapor phase) might explain our observations. Figure 2a shows the transmission electron microscope images (TEM) and high resolution transmission electron microscope images (HRTEM) of Al decorated CNTs grown on Si substrate. The low magnification image resembles a similar morphology as seen in SEM. The TEM observation of the CNTs revealed the formation of MWCNTs consisting of 4−6 graphite layers. It is clear that individual CNTs form bundles with adjacent nanotubes and share a metal tip. Selected area diffraction (SAD) of the particle confirms these particles to be FCC plane (111) of Al. The high magnification image at the point of joint in a bundle confirms the presence of metal particles and several CNTs tangled together. The high magnification image also reveals the nanoparticles embedded in the amorphous carbon layer are in reasonably close contact with the nanotubes, while the other side of the particles is unraveled. The increase in wall diameter due to bundle formation is further verified with Raman measurements. The Al deposition on Inconel shows very similar

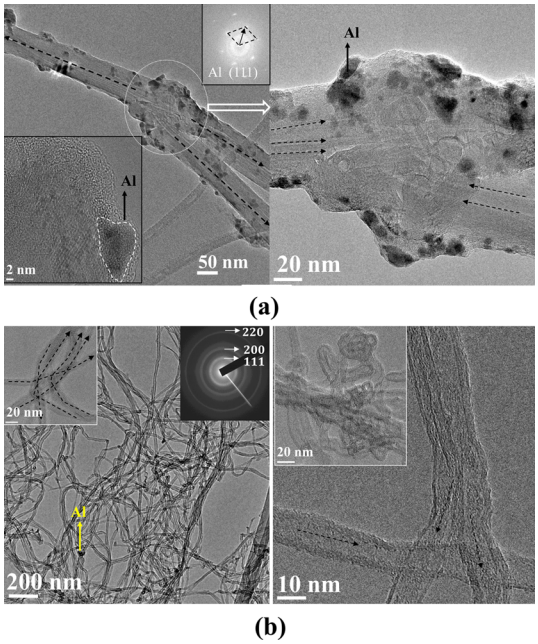

Figure 2. (a) TEM and HRTEM micrograph of the CNTs grown on Si substrate with Al decoration on them. It shows how the CNTs are joined together at the tip, and the high magnification confirms the presence of metal particle. (b) TEM and HRTEM micrograph of the CNTs grown on Inconel.

morphology as shown in Figure 2b. The large area SAD shows the presence of Al planes. The high magnification image shows an increase in diameter with a narrow distribution because of CNTs joining together to form a bundle. The size of the metal nanoparticles was found to be 5−10 nm in diameter.

Raman spectra of the pristine CVD grown CNTs with and without metal deposition are shown in Figure 3a. Raman spectroscopy is the inelastic scattering of light usually associated with absorption or emission of phonons and is rich in information about the structure and chemical bonding of CNTs. Defects and sp^3 hybridized carbon atom give rise to D-band (1340 cm^{-1}) and height of this band is inversely related to the quality of the nanotube (*i.e.*, presence of disorder in the graphitic material). The G-band (~1580 cm^{-1}) is associated with the sp^2 hybridized carbon atom in the nanotube wall and is a good measure of the graphitization of the sample. The G′ or 2D peak (around 2600 cm^{-1}) arises due to two phonon second order scattering process and indicates long-range order in a sample. The ratio of the intensities of the defect or the disorder induced D-band to the symmetry allowed graphitic band or the G-band I_d/I_g characterizes the defect density or degree of disorder in sp^2 hybridized carbon material.[49] The ratio I_{2d}/I_g can be used for identifying the number of walls in the given MWCNT.[50] It is also to be noted that increase in the number of layer leads to a significant decrease in the peak intensity of the 2D peak and this peak becomes hardly distinguishable if the number of layer exceeds 5.[51]

The intensity ratios I_d/I_g and I_{2d}/I_g are given in Table.1. From the results, it is clear that the intensity ratio I_d/I_g of CNTs grown on Si substrate without any metal decoration and with Al decoration was 0.78 and these values are very close to the values reported by Athipalli *et al.*[52] For the CNTs grown on Si substrate with Cu decoration on them this ratio became 0.51. The lower the value of this ratio, lesser the defect, which in turn means lesser amorphous carbon, and greater the degree of graphitic crystallinity. Also, the 2D peak for Al decorated CNTs grown on Inconel was hardly distinguishable and hence the ratio I_{2d}/I_g became zero. As predicted by the work of Ferrari[51] the number of walls must have exceeded five and hence this peak became hardly distinguishable. This was also consistent with TEM, where it is clear that the CNTs join together thereby increasing the number of walls. From the above predictions, it is clear that the CNTs grown on Si with Cu decoration on them have higher graphitic crystallinity with lesser defect. The occurrence of sharp 2D peak on this sample indicates a good long-range order in those samples.

In order to characterize the phase deposited on the CNT forest, the samples are analyzed by X-ray diffraction. Figure 3b shows the representative image of the Al deposition and Cu deposition on Si. In the diffraction pattern we observe reflections at $2\theta = 38°$ and 44° which can be assigned to the (111) and (200) planes of FCC phase of Al. The reflection at $2\theta = 43°$ corresponds to the FCC plane (111) of Cu. These diffraction patterns confirm the presence of metallic particles of Al and Cu and absence of their crystalline oxides. The broadened reflections from the metals clearly reveals the small crystallite size of the metallic particles (~5 nm) supporting observations done with TEM.

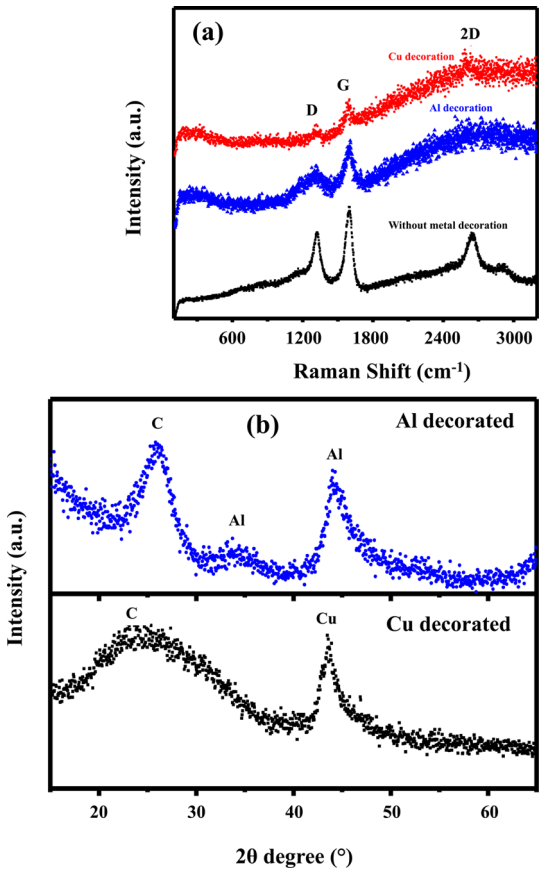

Figure 3. (a) Raman spectra showing 3 distinct peaks [disorder peak D, graphitic peak G and long-range order peak G′ for Si without metal decoration, with Al decoration and Cu decoration]. (b) XRD pattern on Si with Al decoration and XRD pattern on Si with Cu decoration. Al, Cu and C peak clearly prove that there is no oxide formation.

TABLE 1. Values of I_d/I_g and I_{2d}/I_g Ratio for Different Types of CNTs

type of CNTs	I_d/I_g	I_{2d}/I_g
Si substrate	0.78	0.71
Inconel substrate	0.65	0.41
Si substrate/Al decoration	0.78	0.80
Inconel substrate/Al decoration	0.67	0.00
Si substrate/Cu decoration	0.51	0.58
Inconel substrate/Cu decoration	0.66	0.77

The field emission characteristics of the CNTs grown on Si with and without any metal decorations are shown in Figure 4a. The turn on field E_{to}, which is the field required to obtain a current density of 1 μA/cm^2 and the threshold field E_{th}, which is the field required to obtain a current density of 100 μA/cm^2 are summarized in Table 2. The data clearly reveals that Si grown CNTs with Al decoration on them gave the lowest E_{to} and E_{th}, 0.13 and 0.14 V/μm, respectively. One explanation for our low E_{to} and E_{th} for Si grown CNTs with Al decoration on them is due to the lower work function of Al as predicted by Lee *et al.*[53] Similar field emission characteristics were observed for CNTs grown on Inconel

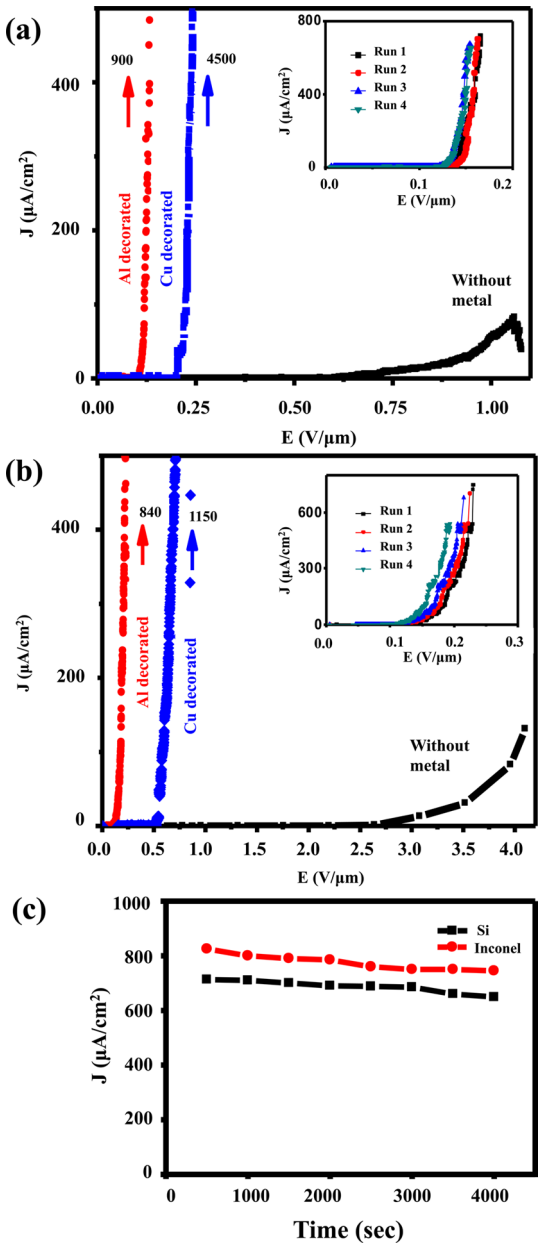

Figure 4. (a) Field emission characteristics of the CNTs grown on Si with and without any metal decorations. It is very clear that the turn on field E_{to} and the threshold field E_{th} are significantly reduced after the metal decoration. Inset in the $J-E$ plot shows emission stability. (b) Field emission characteristics of the CNTs grown on Inconel showing the same phenomena. Inset in the $J-E$ plot shows emission stability. (c) Time trace of current density at the fixed field of 0.15 V/μm for Si grown CNTs and 0.25 V/μm for Inconel grown CNTs, both decorated with Al nanoparticles.

with and without any metal decorations on them. (Figure 4b) The $J-E$ plot was repeatedly measured and it showed good reproducibility. No current saturation was observed over E_{th}.

It is well-known that during field emission, the electrons have to cross two barriers.[54] Barrier 1 is the barrier between the substrate and the CNT and barrier 2 is the barrier between the CNT and the vacuum. Since the Inconel and Al coated Si substrates on which CNTs are

TABLE 2. Values of E_{to} and E_{th} for Different Type of Substrates with and without Metal Decoration

type of CNTs	E_{to} (V/μm)	E_{th} (V/μm)
Si substrate	0.78	2.6
Inconel substrate	1.2	2
Si substrate/Al decoration	0.13	0.14
Inconel substrate/Al decoration	0.14	0.18
Si substrate/Cu decoration	0.19	0.22
Inconel substrate/Cu decoration	0.53	0.58

directly grown have good electrical conductivity, barrier 1 is expected to be reduced substantially enhancing the overall field emission properties of our structures. The measured low contact resistance values for the CNT–substrate interfaces are in agreement with our assumptions as seen in Figure S3 (Supporting Information). Barrier 2 on the other hand has also improved. According to Tanaka *et al.*[55] the presence of amorphous carbon can increase the work function and the E_{th} to a larger extent. One of the explanations for the low E_{th} values for metal decorated CNTs can be due to the reduced amount of amorphous carbon.[45] Although the mechanism that would reduce the amorphous carbon content obtained after Cu decoration is not clear, a plausible explanation might be a partial dissolution of carbon by Cu at the process temperatures applied in the course of evaporation. Another, probably more important, effect that helps electron emission is the promoted electron passage from the nanotubes toward the vacuum through the metal nanoparticles, which may reasonably explain why we observe significant reduction of E_{th} for both metals. The metal nanoparticles form highly conductive electrical paths for the electrons through the amorphous carbon layer (Figure 2a) covering the nanotubes thus ensuring emission centers with clean surface toward the vacuum.

Furthermore, according to Fuji *et al.*[56] the electric field of the bundle is significantly higher at the edge than at the center when compared to the electric field of the flat film which is constant all over the emitter surface. In our samples, due to the metal decoration, the emitter surface is no longer a flat film; instead they are transformed into individual bundles since some of the Al particles went in between the CNTs, thereby increasing the number of edges. The CNTs at the periphery of the bundle formed due to metal decoration acted as a major emission sites. Thus, the excellent field emission property of our emitters can also be attributed to the edge effect.

In addition to the improved field emission $I-V$ characteristics, better emission uniformity is observed from the emission pattern of Al decorated CNTs grown on both Si and Inconel, as shown in the inset of Figure 4. This is because of the increase in the number of available emitters and reduced screening effect. Figure 4c shows the time trace of current density at the fixed field of 0.15 V/μm for Si grown CNTs and 0.25 V/μm for Inconel grown CNTs, both decorated with Al nanoparticles. It was found that there was stable emission for more than an hour due to metal decoration on the CNTs.

CONCLUSIONS

In conclusion, vertically aligned CNTs grown on Al coated Si and Inconel substrates were decorated with Al and Cu particles using a simple and scalable process. The synthesized hybrid structures showed enhanced field emission properties with ultralow turn on and threshold voltages of 0.13 and 0.14 V/μm respectively measured for the Al decorated CNTs grown on Al coated Si. Contact resistance also got reduced substantially in the metal decorated structures which resulted in stable emission for a longer duration without any current degradation. The excellent field emission properties of the metal decorated CNTs can be attributed to the edge effect, reduced screening effect, lower contact resistance, which may pave the road for future devices that require substantially lower bias than the currently existing ones.

METHODS

First the CNTs were grown on Al coated silicon (Si) and Inconel as described elsewhere.[45,57] The grown CNTs were kept inside the CVD chamber with aluminum (Al) sheet of thickness 150 μm over them and the temperature of the system was gradually increased to 700 °C for 10 min and cooled gradually. Since the melting point of Al is 660 °C, it got melted and the CNTs were decorated with Al particles. As the sheet was kept over the array of CNTs, some of the Al particles penetrate in between the CNTs in the array. This process of annealing was done in the presence of Argon (Ar) at a low flow rate. The schematic procedure for the fabrication of metal decorated CNTs is shown in Figure 1c. The same procedure was repeated for the deposition of Cu particles using Cu sheet to obtain Cu decorated CNTs.

The surface morphologies were characterized using scanning electron microscopy (SEM, FEI Quanta 400 ESEM FEG) and high resolution transmission electron microscopy (HRTEM JEOL v2100 F TEM). The content of Al and Cu particles is identified using X-ray diffraction (Rigaku D/Max Ultima II Powder XRD with a Cu Kα source) and Raman spectroscopy (Renishaw in *via* Raman microscope). The area of the sample used was 1 cm^2. After the deposition with metal particles; the sample was transferred to a vacuum chamber with vacuum better than 2×10^{-6} Torr, for field emission measurement. The silicon (Si) and Inconel substrates with CNTs were used as the cathode and indium tin oxide (ITO) coated glass plate as the anode. The cathode and anode mounting stands were machine ground to ensure that they are perfectly parallel. The distance between the cathode and the anode (100 μm) was adjusted using micrometer screw gauge arrangement and a suitable DC voltage (up to 400 V) was supplied using Keithley 2410 high voltage power supply. The electron impedance spectroscopy (EIS) measurements were performed using a two electrode setup with the CNT on the substrate as the working electrode and lithium metal as the

counter/reference electrode. In this, 1 M LiPF6 in 1:1 v/v mixture of ethylene carbonate (EC) and dimethyl carbonate (DMC) are used as the electrolyte and glass microfiber filter membrane as the separator. The EIS measurements were conducted over 70 kHz to 10 mHz by applying a constant dc bias with sinusoidal signal of 10 mV.

Conflict of Interest: The authors declare no competing financial interest.

Acknowledgment. The work done at Rice University has been supported by U.S. Department of Defense: U.S. Air Force Office of Scientific Research for the Project MURI: "Synthesis and Characterization of 3-D Carbon Nanotube Solid Networks" Award No. FA9550-12-1-0035. C.S.T. would like to thank Indian Institute of Science, Bangalore for their support. J.T.-T. acknowledges the support from CONACYT (213780).

Supporting Information Available: A histogram of distance distribution between the CNT bundles and the height of the bundle is included. This is followed by F—N plot for Al decorated CNTs and Cu decorated CNTs grown on both Si and Inconel substrates. Nyquist plots of EIS spectra collected from electrochemical lithium half cell of raw MWCNTs grown without any metal decoration and with Al decoration on CNTs (grown on Si and Inconel substrates) are shown. Information about SEM, TEM and HRTEM characterization of CNTs grown on Silicon and Inconel with Copper decoration on them is available in this section. Images after field emission on metal decorated CNTs are also available. This material is available free of charge *via* the Internet at http://pubs.acs.org.

REFERENCES AND NOTES

1. Planeix, J. M.; Coustel, N.; Coq, B.; Brotons, V.; Kumbhar, P. S.; Dutartre, R.; Geneste, P.; Bernier, P.; Ajayan, P. M. Application of Carbon Nanotubes as Supports in Heterogeneous Catalysis. *J. Am. Chem. Soc.* **1994**, *116*, 7935–7936.
2. Fu, Y.; Zhang, L.; Chen, G. Preparation of a Carbon Nanotube-Copper Nanoparticle Hybrid by Chemical Reduction for Use in the Electrochemical Sensing of Carbohydrates. *Carbon* **2012**, *50*, 2563–2570.
3. Liu, Z.; Lin, X.; Lee, J. Y.; Zhang, W.; Han, M.; Gan, L. M. Preparation and Characterization of Platinum-Based Electrocatalysts on Multiwalled Carbon Nanotubes for Proton Exchange Membrane Fuel Cells. *Langmuir* **2002**, *18*, 4054–4060.
4. Sun, Y.; Wang, H. H. High-Performance, Flexible Hydrogen Sensors That Use Carbon Nanotubes Decorated with Palladium Nanoparticles. *Adv. Mater.* **2007**, *19*, 2818–2823.
5. Li, W.; Liang, C.; Zhou, W.; Qiu, J.; Zhou; Sun, G.; Xin, Q. Preparation and Characterization of Multiwalled Carbon Nanotube-Supported Platinum for Cathode Catalysts of Direct Methanol Fuel Cells. *J. Phys. Chem. B* **2003**, *107*, 6292–6299.
6. Reddy, A.; Ramaprabhu, S. Hydrogen Storage Properties of Nanocrystalline Pt Dispersed Multi-Walled Carbon Nanotubes. *Int. J. Hydrogen Energy* **2007**, *32*, 3998–4004.
7. Kong, J.; Chapline, M. G.; Dai, H. Functionalized Carbon Nanotubes for Molecular Hydrogen Sensors. *Adv. Mater.* **2001**, *13*, 1384–1386.
8. Teo, K. B. K.; Chhowalla, M.; Amaratunga, G. A. J.; Milne, W. I.; Pirio, G.; Legagneux, P.; Wyczisk, F.; Pribat, D.; Hasko, D. G. Field Emission from Dense, Sparse, and Patterned Arrays of Carbon Nanofibers. *Appl. Phys. Lett.* **2002**, *80*, 2011.
9. Stephan, O.; Ajayan, P. M.; Colliex, C.; Redlich, P.; Lambert, J. M.; Bernier, P.; Lefin, P. Doping Graphitic and Carbon Nanotube Structures with Boron and Nitrogen. *Science* **1994**, *266*, 1683–1685.
10. Golberg, D.; Bando, Y.; Bourgeois, L.; Kurashima, K.; Sato, T. Large-Scale Synthesis and HRTEM Analysis of Single-Walled B- and N-Doped Carbon Nanotube Bundles. *Carbon* **2000**, *38*, 2017–2027.
11. Zhang, J.; Yang, C.; Wang, Y.; Feng, T.; Yu, W.; Jiang, J.; Wang, X.; Liu, X. Improvement of the Field Emission of Carbon Nanotubes by Hafnium Coating and Annealing. *Nanotechnology* **2006**, *17*, 257–260.
12. Wei, W.; Jiang, K.; Wei, Y.; Liu, P.; Liu, K.; Zhang, L.; Li, Q.; Fan, S. LaB[sub 6] Tip-Modified Multiwalled Carbon Nanotube as High Quality Field Emission Electron Source. *Appl. Phys. Lett.* **2006**, *89*, 203112.
13. Min, Y.-S.; Bae, E. J.; Park, J. B.; Kim, U. J.; Park, W.; Song, J.; Hwang, C. S.; Park, N. ZnO Nanoparticle Growth on Single-Walled Carbon Nanotubes by Atomic Layer Deposition and a Consequent Lifetime Elongation of Nanotube Field Emission. *Appl. Phys. Lett.* **2007**, *90*, 263104.
14. Green, J. M.; Dong, L.; Gutu, T.; Jiao, J.; Conley, J. F.; Ono, Y. ZnO-Nanoparticle-Coated Carbon Nanotubes Demonstrating Enhanced Electron Field-Emission Properties. *J. Appl. Phys.* **2006**, *99*, 094308.
15. Liu, C.; Kim, K. S.; Baek, J.; Cho, Y.; Han, S.; Kim, S.-W.; Min, N.-K.; Choi, Y.; Kim, J.-U.; Lee, C. J. Improved Field Emission Properties of Double-Walled Carbon Nanotubes Decorated with Ru Nanoparticles. *Carbon* **2009**, *47*, 1158–1164.
16. Jonge, N. de; Allioux, M.; Doytcheva, M.; Kaiser, M.; Teo, K. B. K.; Lacerda, R. G.; Milne, W. I. Characterization of the Field Emission Properties of Individual Thin Carbon Nanotubes. *Appl. Phys. Lett.* **2004**, *85*, 1607.
17. Han, S.; Ihm, J. First-Principles Study of Field Emission of Carbon Nanotubes. *Phys. Rev. B: Condens. Matter Mater. Phys.* **2002**, *66*, 241402.
18. Kim, H.-S.; Lee, H.; Han, K.-S.; Kim, J.-H.; Song, M.-S.; Park, M.-S.; Lee, J.-Y.; Kang, J.-K. Hydrogen Storage in Ni Nanoparticle-Dispersed Multiwalled Carbon Nanotubes. *J. Phys. Chem. B* **2005**, *109*, 8983–8986.
19. Kim, J.-Y.; Jeong, T.; Baik, C.-W.; Park, S. H.; Han, I.; Kim, G.-H.; Yu, S. Field-Emission Performance and Structural Change Mechanism of Multiwalled Carbon Nanotubes by Oxygen Plasma Treatment. *Thin Solid Films* **2013**, *547*, 202–206.
20. Choi, H.; Ji Shin, Y.; Il Cha, S.; Ho Kang, I.; Bahng, W. Enhanced Field-Emission Capacity by Density Control of a CNT Cathode Using Post-Plasma Treatment. *Solid State Commun.* **2013**, *171*, 50–54.
21. Xiao, L.; Liu, P.; Liu, L.; Jiang, K.; Feng, X.; Wei, Y.; Qian, L.; Fan, S.; Zhang, T. Barium-Functionalized Multiwalled Carbon Nanotube Yarns as Low-Work-Function Thermionic Cathodes. *Appl. Phys. Lett.* **2008**, *92*, 153108.
22. Lyth, S. M.; Hatton, R. A.; Silva, S. R. P. Efficient Field Emission from Li-Salt Functionalized Multiwall Carbon Nanotubes on Flexible Substrates. *Appl. Phys. Lett.* **2007**, *90*, 013120.
23. Jin, F.; Liu, Y.; Day, C. M.; Little, S. A. Enhanced Electron Emission from Functionalized Carbon Nanotubes with a Barium Strontium Oxide Coating Produced by Magnetron Sputtering. *Carbon* **2007**, *45*, 587–593.
24. Feng, M.; Sun, R.; Zhan, H.; Chen, Y. Decoration of Carbon Nanotubes with CdS Nanoparticles by Polythiophene Interlinking for Optical Limiting Enhancement. *Carbon* **2010**, *48*, 1177–1185.
25. Wang, W.; Serp, P.; Kalck, P.; Silva, C. G.; Faria, J. L. Preparation and Characterization of Nanostructured MWCNT-TiO_2 Composite Materials for Photocatalytic Water Treatment Applications. *Mater. Res. Bull.* **2008**, *43*, 958–967.
26. Haremza, J. M.; Hahn, M. A.; Krauss, T. D.; Chen, S.; Calcines, J. Attachment of Single CdSe Nanocrystals to Individual Single-Walled Carbon Nanotubes. *Nano Lett.* **2002**, *2*, 1253–1258.
27. Huang, C.-S.; Yeh, C.-Y.; Chang, Y.-H.; Hsieh, Y.-M.; Ku, C.-Y.; Lai, Q.-T. Field Emission Properties of CNT—ZnO Composite Materials. *Diamond Relat. Mater.* **2009**, *18*, 452–456.
28. Yang, M.; Liang, T.; Peng, Y.; Chen, Q. Synthesis and Characterization of a Nanocomplex of ZnO Nanoparticles Attached to Carbon Nanotubes. *Acta Phys.-Chim. Sin.* **2007**, *23*, 145–151.
29. An, G.; Na, N.; Zhang, X.; Miao, Z.; Miao, S.; Ding, K.; Liu, Z. SnO_2 /carbon Nanotube Nanocomposites Synthesized in Supercritical Fluids: Highly Efficient Materials for Use as a Chemical Sensor and as the Anode of a Lithium-Ion Battery. *Nanotechnology* **2007**, *18*, 435707.

30. Zhai, L.; Wei, Z.; Yang, Z.; Ni, X. Polymerization Initiated by ZnS Nanocrystals Anchored on Carbon Nanotubes. *Mater. Lett.* **2010**, *64*, 531–533.
31. Cho, N.; Roy Choudhury, K.; Thapa, R. B.; Sahoo, Y.; Ohulchanskyy, T.; Cartwright, A. N.; Lee, K.-S.; Prasad, P. N. Efficient Photodetection at IR Wavelengths by Incorporation of PbSe−Carbon-Nanotube Conjugates in a Polymeric Nanocomposite. *Adv. Mater.* **2007**, *19*, 232–236.
32. Li, C.; Ding, S.; Lei, W.; Zhang, X.; Wang, B. Enhanced Field Emission from Vertically Aligned Carbon Nanotubes on Metal Mesh Electrode. *Appl. Surf. Sci.* **2013**, *285*, 505–508.
33. Zuo, Y.; Ren, Y.; Wang, Z.; Han, X.; Xi, L. Enhanced Field Emission and Hysteresis Characteristics of Aligned Carbon Nanotubes with Ti Decoration. *Org. Electron.* **2013**, *14*, 2306–2314.
34. Pandey, A.; Prasad, A.; Moscatello, J. P.; Engelhard, M.; Wang, C.; Yap, Y. K. Very Stable Electron Field Emission from Strontium Titanate Coated Carbon Nanotube Matrices with Low Emission Thresholds. *ACS Nano* **2013**, *7*, 117–125.
35. Zanin, H.; May, P. W.; Hamanaka, M. H. M. O.; Corat, E. J. Field Emission from Hybrid Diamond-like Carbon and Carbon Nanotube Composite Structures. *ACS Appl. Mater. Interfaces* **2013**, *5*, 12238–12243.
36. Fan, Y. C.; Liu, Y. M.; Chen, Y. C.; Sung, Y.; Ger, M. D. Carbon Nanotube Field Emission Cathodes Fabricated with Chemical Displacement Plating. *Appl. Surf. Sci.* **2009**, *255*, 7753–7758.
37. Chen, Y.; Jiang, H.; Li, D.; Song, H.; Li, Z.; Sun, X.; Miao, G.; Zhao, H. Improved Field Emission Performance of Carbon Nanotube by Introducing Copper Metallic Particles. *Nanoscale Res. Lett.* **2011**, *6*, 537.
38. Nilsson, L.; Groening, O.; Emmenegger, C.; Kuettel, O.; Schaller, E.; Schlapbach, L.; Kind, H.; Bonard, J.-M.; Kern, K. Scanning Field Emission from Patterned Carbon Nanotube Films. *Appl. Phys. Lett.* **2000**, *76*, 2071.
39. Bonard, J.-M.; Dean, K.; Coll, B.; Klinke, C. Field Emission of Individual Carbon Nanotubes in the Scanning Electron Microscope. *Phys. Rev. Lett.* **2002**, 89.
40. Bonard, J.-M.; Weiss, N.; Kind, H.; Stöckli, T.; Forró, L.; Kern, K.; Châtelain, A. Tuning the Field Emission Properties of Patterned Carbon Nanotube Films. *Adv. Mater.* **2001**, *13*, 184–188.
41. Bittencourt, C.; Ke, X.; Van Tendeloo, G.; Thiess, S.; Drube, W.; Ghijsen, J.; Ewels, C. P. Study of the Interaction between Copper and Carbon Nanotubes. *Chem. Phys. Lett.* **2012**, *535*, 80–83.
42. Gingery, D.; Bühlmann, P. Formation of Gold Nanoparticles on Multiwalled Carbon Nanotubes by Thermal Evaporation. *Carbon* **2008**, *46*, 1966–1972.
43. Charlier, J.-C.; Arnaud, L.; Avilov, I. V.; Delgado, M.; Demoisson, F.; Espinosa, E. H.; Ewels, C. P.; Felten, A.; Guillot, J.; Ionescu, R.; *et al.* Carbon Nanotubes Randomly Decorated with Gold Clusters: From Nano ^{2} Hybrid Atomic Structures to Gas Sensing Prototypes. *Nanotechnology* **2009**, *20*, 375501.
44. Muratore, C.; Reed, A. N.; Bultman, J. E.; Ganguli, S.; Cola, B. A.; Voevodin, A. A. Nanoparticle Decoration of Carbon Nanotubes by Sputtering. *Carbon* **2013**, *57*, 274–281.
45. Sridhar, S.; Ge, L.; Tiwary, C. S.; Hart, A. C.; Ozden, S.; Kalaga, K.; Lei, S.; Sridhar, S. V.; Sinha, R. K.; Harsh, H.; *et al.* Enhanced Field Emission Properties from CNT Arrays Synthesized on Inconel Superalloy. *ACS Appl. Mater. Interfaces* **2014**, 1986–1991.
46. Katayama, M.; Lee, K.-Y.; Honda, S.; Hirao, T.; Oura, K. Ultra-Low-Threshold Field Electron Emission from Pillar Array of Aligned Carbon Nanotube Bundles. *Jpn. J. Appl. Phys.* **2004**, *43*, L774–L776.
47. Suh, J. S.; Jeong, K. S.; Lee, J. S.; Han, I. Study of the Field-Screening Effect of Highly Ordered Carbon Nanotube Arrays. *Appl. Phys. Lett.* **2002**, *80*, 2392.
48. Ren, H.; Yang, L.; Zhang, Y. Numerical Calculations on the Field Emission of Carbon Nanotubes. *J. Phys.: Conf. Ser.* **2013**, *418*, 012007.
49. Tuinstra, F. Raman Spectrum of Graphite. *J. Chem. Phys.* **1970**, *53*, 1126.
50. Saito, R.; Hofmann, M.; Dresselhaus, G.; Jorio, A.; Dresselhaus, M. S. Raman Spectroscopy of Graphene and Carbon Nanotubes. *Adv. Phys.* **2011**, *60*, 413–550.
51. Ferrari, A. C. Raman Spectroscopy of Graphene and Graphite: Disorder, Electron−Phonon Coupling, Doping and Nonadiabatic Effects. *Solid State Commun.* **2007**, *143*, 47–57.
52. Atthipalli, G.; Wang, H.; Gray, J. L. Catalyst-Assisted Vertical Growth of Carbon Nanotubes on Inconel Coated Commercial Copper Foil Substrates *versus* Sputtered Copper Films. *Appl. Surf. Sci.* **2013**, *273*, 515–519.
53. Lee, D. H.; Lee, J. A.; Lee, W. J.; Choi, D. S.; Lee, W. J.; Kim, S. O. Facile Fabrication and Field Emission of Metal-Particle-Decorated Vertical N-Doped Carbon Nanotube/Graphene Hybrid Films. *J. Phys. Chem. C* **2010**, *114*, 21184–21189.
54. Gadzuk, J.; Plummer, E. Field Emission Energy Distribution (FEED). *Rev. Mod. Phys.* **1973**, *45*, 487–548.
55. Tanaka, H.; Akita, S.; Pan, L.; Nakayama, Y. Barrier Effect on Field Emission from Stand-Alone Carbon Nanotube. *Jpn. J. Appl. Phys.* **2004**, *43*, 864–867.
56. Fujii, S.; Honda, S.; Machida, H.; Kawai, H.; Ishida, K.; Katayama, M.; Furuta, H.; Hirao, T.; Oura, K. Efficient Field Emission from an Individual Aligned Carbon Nanotube Bundle Enhanced by Edge Effect. *Appl. Phys. Lett.* **2007**, *90*, 153108.
57. Collins, P. G.; Zettl, A. Unique Characteristics of Cold Cathode Carbon-Nanotube-Matrix Field Emitters. *Phys. Rev. B: Condens. Matter Mater. Phys.* **1997**, *55*, 9391–9399.